Noname manuscript No.
(will be inserted by the editor)

An a posteriori error estimator for *hp*-adaptive continuous Galerkin methods for photonic crystal applications

Stefano Giani

Abstract In this paper we propose and analyse an error estimator suitable for *hp*-adaptive continuous finite element methods for computing the band structure and the isolated modes of 2D photonic crystal (PC) applications.

The error estimator that we propose is based on the residual of the discrete problem and we show that it leads to very fast convergence in all considered examples when used with *hp*-adaptive refinement techniques.

In order to show the flexibility and robustness of the error estimator we present an extensive collection of numerical experiments inspired by real applications. In particular we are going to consider PCs with point defects, PCs with line defects, bended waveguides and semi-infinite PCs.

Keywords eigenvalue problem · finite element method · *hp*-adaptivity · a posteriori error estimator · photonic crystals

Mathematics Subject Classification (2000) 65N25 · 65N30 · 65N50

1 Introduction

The purpose of this work is to demonstrate that the presented error estimator can improve the study of wave propagation in photonic crystal applications by reducing the computational cost when used with *hp*-adaptivity. All the photonic crystal examples analysed in this work are constructed starting with a periodic medium, then defects are introduced to enhance the properties of the crystal. All of the resulting geometries of photonic crystals that were used are inspired by real applications.

Photonic crystals have many applications, for example, in optical communications, filters, lasers, switches and optical transistors; see [21,33,23,3] for

S. Giani
School of Mathematical Sciences, University of Nottingham, University Park, Nottingham, NG7 2RD, UK. E-mail: stefano.giani@nottingham.ac.uk

an introduction to photonic crystals and see [20,27] for an introduction to applications.

All problems considered in this work are defined on a rectangular domain Ω and they can be written in the following form for different choices of the functional space $\mathcal{H}$ and the bounded set $\mathcal{K}$ in $\mathbb{R}^2$: *seek eigenpairs of the form* $(\lambda, u) \in \mathbb{R} \times \mathcal{H}$*, with* u *appropriately normalised, such that*

$$\int_\Omega ((\nabla + i\boldsymbol{\kappa})v)^* \mathcal{A}(\nabla + i\boldsymbol{\kappa})u \;=\; \lambda \int_\Omega \mathcal{B}u\bar{v} \quad \text{for all } v \in \mathcal{H}, \tag{1}$$

where the parameter $\boldsymbol{\kappa}$ varies in the bounded set $\mathcal{K}$ and where * denotes Hermitian transpose. Here, the (generally) matrix-valued function $\mathcal{A}$ is real, symmetric and uniformly bounded and positive definite, i.e. there exist constants $\underline{a}$ and $\overline{a}$ such that

$$0 < \;\underline{a}\; \leq\; \xi^* \mathcal{A}(x)\xi \;\leq\; \overline{a} \quad \text{for all } \xi \in \mathbb{R}^2 \text{ with } |\xi| = 1 \text{ and all} \quad x \in \Omega. \tag{2}$$

The scalar function $\mathcal{B}$ is real and uniformly bounded above and below by positive constants $\underline{b}$ and $\overline{b}$, i.e.,

$$0 \;<\; \underline{b} \;\leq\; \mathcal{B}(x) \;\leq\; \overline{b} \quad \text{for all } x \in \Omega. \tag{3}$$

We allow for $\mathcal{A}$ and $\mathcal{B}$ to be in general discontinuous but only under the condition that the jumps of the coefficients are aligned with the meshes. Moreover, in this work we only consider PCs with a finite number of materials, so the possible values of $\mathcal{A}$ and $\mathcal{B}$ are finite as well.

As explained in the next section, equation (1) describes several different problems related to PCs. In this paper we are going to consider PCs with point defects, PCs with line defects, bended waveguides and semi-infinite PCs.

Equation (1) is derived from Maxwell's equations which govern the propagation of light in PCs. In 2D PCs, the 3D Maxwell's equations reduce to a 2D one-component wave equation, which determines either the electric field or the magnetic field. Depending on the considered kind of PC, different approaches can be used to further reduce the 2D wave equation on an infinite domain to a family of eigenvalue problems on bounded domains. All such approaches involve the Floquet transform [23,22] to exploit the periodicity of the crystal.

A very popular practical numerical method for PCs is the Fourier spectral method (also called the "plane-wave expansion method") [32,21,10,30,31]. This method exploits the periodicity in the PC and uses modern highly tuned FFT algorithms to obtain fast implementations. However, the overall rate of convergence of approximate spectra to true spectra is slow because the jumps in the dielectric destroy the exponential accuracy which is achieved by Fourier spectral methods for smooth problems.

Instead our approach is based on adaptive finite element methods because they provide flexible solvers for PDE eigenvalue problems and they are able to deal optimally with heterogeneous media. There are already a number of papers about low order finite element methods for PCs [5,9,11,12] and most recently there has been considerable interest in h, p and hp methods [19,14,

25,35,34]. Accurate computations based on *a priori hp* refinement strategies are shown in [35,34]. However, as far as we are aware, until now no one has used *hp*-adaptivity based on a posteriori error estimates on these problems with continuous Galerkin methods.

The outline of the paper is as follows. The next section - §2 - briefly describes how problem (1) is derived from Maxwell's equations. Then in §3 we characterize the finite element spaces and introduce the discrete version of problem (1). In the following section §4 the error estimator is presented together with the proof of reliability. Finally in §5 we present all the numerical results.

2 Photonic crystal eigenvalue problems

In general, PCs are of practical interest because of the properties of their spectra which can be exploited in many applications. The most useful properties are the presence of band-gaps - i.e., monochromatic electromagnetic waves of certain frequencies may not propagate inside the crystal - and possibly the presence of trapped modes within the gaps.

The mathematical development (see e.g. [23]) begins with time harmonic Maxwell's equations with eigenvalue ω

$$\begin{array}{ll} \nabla \times \mathbf{E}_\omega = -\frac{i\omega}{c}\mu \mathbf{H}_\omega, & \nabla \cdot \mu \mathbf{H}_\omega = 0 \ , \\ \nabla \times \mathbf{H}_\omega = \frac{i\omega}{c}\varepsilon \mathbf{E}_\omega \ , & \nabla \cdot \varepsilon \mathbf{E}_\omega = 0 \ , \end{array} \tag{4}$$

where ω is the frequency, $\mathbf{E}_\omega$ is the electric field, $\mathbf{H}_\omega$ is the magnetic field, ε and μ are, respectively, the dielectric permittivity and magnetic permeability tensors, and c is the speed of light in vacuum. We assume that the medium is periodic in the (x, y) plane and that it is constant in the third (z) direction. Furthermore we assume that the material is non-magnetic (so $\mu = 1$). If we only consider $\mathbf{E}_\omega = \mathbf{E}_\omega(x, y)$ and $\mathbf{H}_\omega = \mathbf{H}_\omega(x, y)$ then problem (4) splits naturally into two independent problems, called transverse magnetic (TM) and transverse electric (TE) modes, as explained in [23]:

$$\Delta u_\omega + \frac{\omega^2}{c^2}\varepsilon u_\omega = 0 \quad \text{(TM case)} \ , \tag{5}$$

$$\nabla \cdot \frac{1}{\varepsilon}(\nabla u_\omega) + \frac{\omega^2}{c^2} u_\omega = 0, \quad \text{(TE case)} \ . \tag{6}$$

Both problems (5) and (6) may be written in the abstract form as that of seeking (λ, u) with $u \neq 0$ such that

$$\nabla \cdot (\mathcal{A}\nabla u) + \lambda \mathcal{B} u \ = \ 0 \ . \tag{7}$$

Since $\mathcal{A}$ or $\mathcal{B}$ may be discontinuous, (7) has to be understood in an appropriate weak form. So far (7) is posed over all of $\mathbb{R}^2$, with periodic data. Problem (7) is difficult to solve numerically because it is posed on an unbounded domain and because such problem has spectrum formed by bands of essential spectrum. In

order to make the problem easier to solve, we use the Floquet transform [23] to derive a family of problems with discrete spectra.

A 2D periodic medium can be described using a lattice $L := \{\mathbf{R} = n_1\mathbf{r}_1 + n_2\mathbf{r}_2 \ , \ n_1, n_2 \in \mathbb{Z}\}$, where $\{\mathbf{r}_1, \mathbf{r}_2\}$ is a basis for $\mathbb{R}^2$. The (Wigner-Seitz) primitive cell for L is the set Ω_C of all points in $\mathbb{R}^2$ which are closer to $\mathbf{0}$ than to any other point in L [4]. When $\overline{\Omega_C}$ is translated through all $\mathbf{R} \in L$, we obtain a covering of $\mathbb{R}^2$ with overlap of measure 0. The reciprocal lattice for L is the lattice $\hat{L}$ generated by a basis $\{\mathbf{k}_1, \mathbf{k}_2\}$, chosen so that $\mathbf{r}_i \cdot \mathbf{k}_j = 2\pi\delta_{i,j}$, $i, j = 1, 2$, where $\delta_{i,j}$ is the Kronecker delta and the primitive cell for the reciprocal lattice is called the first Brillouin zone, which we denote here by $\mathcal{K}_{2\mathrm{D},\Omega_C}$ [4]. For example, if L is the square lattice generated by $\{\mathbf{e}_1, \mathbf{e_2}\}$ (where $\mathbf{e}_i$ are the standard basis vectors in $\mathbb{R}^2$), then $\Omega_C = (-0.5, 0.5)^2$, $\hat{L}$ is generated by $\{2\pi\mathbf{e}_1, 2\pi\mathbf{e_2}\}$ and the first Brillouin zone is $\mathcal{K}_{2\mathrm{D},\Omega_C} = (-\pi, +\pi)^2$.

The Floquet transform [23] may then be used to show the equivalence of problem (7) to a family of problems on the primitive cell Ω_C with periodic boundary conditions parametrized by quasimomentum $\kappa \in \mathcal{K}_{2\mathrm{D},\Omega_C}$. This is the family

$$(\nabla + i\boldsymbol{\kappa}) \cdot \mathcal{A}(\nabla + i\boldsymbol{\kappa})\tilde{u} + \lambda B\tilde{u} \ = \ 0 \quad \text{on } \Omega_C, \quad \boldsymbol{\kappa} \in \mathcal{K}_{2\mathrm{D},\Omega_C} \ , \tag{8}$$

where $\tilde{u}$ satisfies periodic boundary conditions and it is the Floquet transform of u and λ is the corresponding eigenvalue which now depends on κ - a rigorous derivation can be found for example in [8]. This equation should again be understood in the weak form. In order to recover the spectrum of problem (7), it is sufficient to compute the closure of the union of all the spectra of the problems in the family (8) for all $\kappa \in \mathcal{K}_{2\mathrm{D},\Omega_C}$, and these problems have discrete and real spectra [23]. Writing (8) in weak form gives precisely (1).

Equation (8) models an infinite PC with periodic data. In order to analyse the case of PCs with defects such as point defects, line defects and bends, we modify the model problem as described in the super-cell framework [36]. In this framework the domain of the problem is not anymore a single cell, but a bigger portion of the periodic medium containing also defects, see Figures 1(a), 1(b) and 1(c) for examples of such domains for different kind of PC applications. Denoting by Ω_S the super-cell we then have the family of problems with periodic boundary conditions

$$(\nabla + i\boldsymbol{\kappa}) \cdot \mathcal{A}(\nabla + i\boldsymbol{\kappa})\tilde{u} + \lambda B\tilde{u} \ = \ 0 \quad \text{on } \Omega_S, \quad \boldsymbol{\kappa} \in \mathcal{K}_{2\mathrm{D},\Omega_S} \ , \tag{9}$$

where $\mathcal{K}_{2\mathrm{D},\Omega_S}$ is the first Brillouin zone corresponding to Ω_S.

In order to derive the model problem for a semi-infinite PC we have to proceed in a different way. Assuming that the PC fills only the half of the space $\mathbb{R}^2$ with $x > 0$, see Figure 1(d). Then we need to apply the Floquet transform to (7) only in the y-direction. In this way the resulting problem is:

$$(\nabla + i\boldsymbol{\kappa}) \cdot \mathcal{A}(\nabla + i\boldsymbol{\kappa})\tilde{u} + \lambda B\tilde{u} \ = \ 0 \quad \text{on } \hat{\Omega}, \quad \boldsymbol{\kappa} \in \mathcal{K}_{1\mathrm{D},\hat{\Omega}} \ ,$$

where $\tilde{u}$ satisfies periodic boundary conditions on the horizontal boundaries of $\hat{\Omega} := \mathbb{R} \times [-0.5, +0.5]$ and where the corresponding first Brillouin zone is

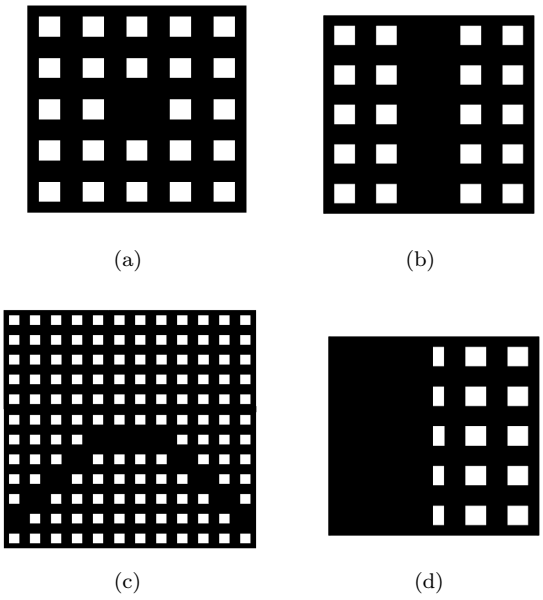

Fig. 1 Examples of super-cells for different PC configurations: (a) PC with point defect. (b) PC with line defect. (c) V-bend wave guide. (d) Portion of a semi-infinite PC.

$\mathcal{K}_{1\mathrm{D},\hat{\Omega}} := \{0\}\times[-\pi,+\pi]$. Since the domain $\hat{\Omega}$ is still unbounded, it is necessary to truncate the domain $\hat{\Omega}$ in the x-direction far enough away from the surface of the crystal. The resulting domain Ω_T is of rectangular shape with periodic boundary conditions in the y-direction and homogeneous Dirichlet boundary conditions in the x-direction and the resulting problem is:

$$(\nabla + i\boldsymbol{\kappa})\cdot\mathcal{A}(\nabla + i\boldsymbol{\kappa})\tilde{u} + \lambda B\tilde{u} \;=\; 0 \quad \text{on } \Omega_T, \qquad \boldsymbol{\kappa}\in\mathcal{K}_{1\mathrm{D},\Omega_T}\ , \tag{10}$$

where $\mathcal{K}_{1\mathrm{D},\Omega_T} \equiv \mathcal{K}_{1\mathrm{D},\hat{\Omega}}$. The effects of the truncation of the domain on self-adjoint problems with potential has been fully analysed in [26]. The results presented in such work show that enlarging the domain, the eigenvalues of the truncated problem converge to the eigenvalues of the unbounded problem. In view of that it seems plausible that for $-(\nabla+i\boldsymbol{\kappa})\cdot\mathcal{A}(\nabla+i\boldsymbol{\kappa})\tilde{u}$ in problem (10), which can be seen as a self-adjoint operator with zero potential, the surface modes, which are confined in a narrow strip region containing the surface of the crystal, still exist in the spectrum of the truncated problem and that, enlarging the domain, such modes of the truncated problem may converge to the surface modes of the unbounded problem.

3 Discrete eigenvalue problems

Throughout $L^2(\Omega)$ denotes the usual space of square integrable complex valued functions equipped with the weighted norm

$$\|g\|_{0,\mathcal{B}} \;=\; b(g,g)^{1/2}\;, \quad b(g,w) := \int_\Omega \mathcal{B} g \bar{w}\;, \tag{11}$$

where $\Omega = \Omega_C, \Omega_S, \Omega_T$. $H^1(\Omega)$ denotes the usual space of functions in $L^2(\Omega)$ with square integrable gradient, the H^1-norm is denoted $\|g\|_1$ and $H^1_\pi(\Omega)$ denotes the subspace of functions in $g \in H^1(\Omega)$ which satisfy periodic boundary conditions on $\partial\Omega$. Furthermore we denote with $H^1_{0,\pi}(\Omega)$ the subspace of functions in $g \in H^1(\Omega)$ which satisfy periodic boundary conditions on the horizontal boundaries of Ω, where Ω is supposed to be of rectangular shape, and homogeneous Dirichlet on the vertical boundaries of Ω. When we want to restrict these norms to a measurable subset $S \subseteq \Omega$, we write $\|g\|_{0,\mathcal{B},S}$, $\|g\|_{1,S}$, etc.

Problem (1) can be rewritten as: *for $\boldsymbol{\kappa} \in \mathcal{K}$ seek eigenpairs of the form $(\lambda_j, u_j) \in \mathbb{R} \times \mathcal{H}$ such that*

$$\left.\begin{array}{ll} a_\kappa(u_j, v) = \lambda_j\; b(u_j, v)\;, & \text{for all} \quad v \in \mathcal{H} \\ \|u_j\|_{0,\mathcal{B}} \;= 1 & \end{array}\right\} \tag{12}$$

where

$$a_\kappa(u,v) := \int_\Omega ((\nabla + i\boldsymbol{\kappa})v(x))^* \mathcal{A}(x)((\nabla + i\boldsymbol{\kappa})u(x))\;. \tag{13}$$

Depending on the problem under consideration different definitions for Ω, $\mathcal{H}$ and $\mathcal{K}$ should be applied. In particular for problems with point defects, line defects and bended waveguides, we have from (9) that $\mathcal{H} := H^1_\pi(\Omega_S)$ and $\mathcal{K} := \mathcal{K}_{2\mathrm{D},\Omega_S}$. On the other hand for semi-infinite crystals we have from (10) that $\mathcal{H} := H^1_{0,\pi}(\Omega_T)$ and $\mathcal{K} := \mathcal{K}_{1\mathrm{D},\Omega_T}$.

Now, to discretize (12), let $\mathcal{T}_n\;, n = 1, 2, \ldots$ denote a family of conforming, shape-regular triangulations [1]. In all problems considered in this work we impose in some parts or along the all boundary of the domain periodic boundary conditions. The effect of imposing periodic boundary conditions is that opposite edges of the domain are identified, this means that the number of nodes and the positions of them should coincide on identified edges in order to keep the finite element method conforming. These meshes may be computed adaptively. With h_τ denoting the diameter of element τ, we define $h_n^{\max} := \max_{\tau\in\mathcal{T}_n}\{h_\tau\}$. We store the elemental diameters in the mesh size vector $\underline{h} = \{\, h_\tau \,:\, \tau \in \mathcal{T}_n \,\}$.

The set $\mathcal{F}(\mathcal{T}_n)$ contains all the internal mesh edges and all the boundary edges where periodic boundary conditions are imposed. Because of the presence of periodic boundary conditions, not all the edges along the boundary of Ω have to be considered as boundary edges, therefore some of the edges of the mesh along $\partial\Omega$ are actually treated as interior edges. In this case the second element sharing the edge is on the opposite side of the domain. The diameter

of an edge f is denoted by h_f, similarly we denote with $\mathcal{F}(\tau)$ the set of all edges of the element τ.

In order to define the finite element space on $\mathcal{T}_n$, we begin by introducing polynomial spaces on elements. To that end, let $\tau \in \mathcal{T}_n$ be an element, we set $\mathcal{P}_p(\tau)$ to be the set of polynomials on the element τ of total degree less than or equal to p. Then, we assign a polynomial degree $p_\tau \geq 1$ with each element τ of the mesh $\mathcal{T}_n$. We then introduce the degree vector $\underline{p} = \{ p_\tau \,:\, \tau \in \mathcal{T}_n \}$. We assume that $\underline{p}$ is of bounded local variation, i.e. there is a constant $\varrho \geq 1$, independent of the mesh $\mathcal{T}_n$ under consideration, such that $\varrho^{-1} \leq p_\tau / p_{\tau'} \leq \varrho$ for any pair of neighboring elements $\tau, \tau' \in \mathcal{T}_n$. We finally denote by p_f the maximum of the order of polynomials of the two elements sharing the face $f \in \mathcal{F}(\mathcal{T}_n)$.

For a partition $\mathcal{T}_n$ of Ω and a polynomial degree vector $\underline{p}$ on $\mathcal{T}_n$, we define the finite element spaces of continuous functions by

$$S_{\underline{p}}(\mathcal{T}_n, \Omega_S) = \{ v \in H^1_\pi(\Omega_S) \,:\, v|_\tau \in \mathcal{P}_{p_\tau}(\tau),\ \tau \in \mathcal{T}_n \}, \tag{14}$$

for the problems on super-cells and by

$$S_{\underline{p}}(\mathcal{T}_n, \Omega_T) = \{ v \in H^1_{0,\pi}(\Omega_T) \,:\, v|_\tau \in \mathcal{P}_{p_\tau}(\tau),\ \tau \in \mathcal{T}_n \}, \tag{15}$$

for the semi-infinite crystal problem. Where it is not necessary to distinguish between these two cases, we denote the finite element space with $S_{\underline{p}}(\mathcal{T}_n, \Omega)$.

The discrete approximation of problem (12) is: *seek eigenpairs of the form* $(\lambda_{j,n}, u_{j,n}) \in \mathbb{R} \times S_{\underline{p}}(\mathcal{T}_n, \Omega)$ *such that*

$$\left.\begin{array}{ll} a_\kappa(u_{j,n}, v_n) = \lambda_{j,n}\, b(u_{j,n}, v_n)\ , & \text{for all} \quad v_n \in S_{\underline{p}}(\mathcal{T}_n, \Omega) \\ \|u_{j,n}\|_{0,\mathcal{B}} = 1 & \end{array}\right\} \tag{16}$$

It is easy to see that a_κ is a Hermitian form which is bounded independently of $\kappa \in \mathcal{K}$ on $H^1(\Omega)$, where Ω is either Ω_C, Ω_S or Ω_T. Moreover by the positive definiteness of $\mathcal{A}$ assumed in (2), we have

$$a_\kappa(u,u) \ \geq\ \underline{a} \int_\Omega |(\nabla + i\kappa)u|^2 \geq 0\ , \quad \text{for all } u \in \mathcal{H}\ , \tag{17}$$

where $\mathcal{H}$ is either $H^1_\pi(\Omega_C)$, $H^1_\pi(\Omega_S)$ or $H^1_{\pi,0}(\Omega_T)$. Thus the spectrum of (12) is real and non-negative

However $a_\kappa(u,u)$ on $H^1_\pi(\Omega_C)$ and on $H^1_\pi(\Omega_S)$ is not always strictly positive (for $u \neq 0$), since if $\kappa = (0,0)$ then $a_\kappa(1,1) = 0$. Thus we introduce the shifted Hermitian form:

$$(u,v)_{\kappa,\mathcal{A},\mathcal{B}} \ :=\ a_\kappa(u,v) + \ \sigma\ b(u,v)\ , \quad \text{for all } u, v \in H^1_\pi(\Omega)\ , \tag{18}$$

with a fixed shift $\sigma := \max_{\kappa\in\mathcal{K}} |\kappa|^2 \underline{a}/\underline{b} \ +\ 1$. The following result shows that the shifted form is coercive on $H^1_\pi(\Omega)$ (i.e., $(u,u)_{\kappa,A,B}/\|u\|_1^2$ is bounded below by a positive constant for all $u \neq 0$). The norm induced by this shifted form is used in the theory below, but it is never used in computations.

Lemma 1 *The sesquilinear form* $(\cdot,\cdot)_{\kappa,A,B}$ *is an inner product on* $H^1_\pi(\Omega)$. *(We denote the induced norm by* $\|\cdot\|_{\kappa,\mathcal{A},\mathcal{B}}$*.)*

The proof of such result can be found in [19, Lemma 2.1].

Remark 1 In order to keep the exposition as simple as possible, we treated also the problem on semi-infinite crystals in the same way using the shifted Hermitian form.

Problem (12) can be rewritten using the Hermitian form $(\cdot,\cdot)_{\kappa,\mathcal{A},\mathcal{B}}$ as: *for* $\boldsymbol{\kappa} \in \mathcal{K}$ *seek eigenpairs of the form* $(\zeta_j, u_j) \in \mathbb{R} \times \mathcal{H}$ *such that*

$$\left.\begin{array}{ll} (u_j, v)_{\kappa,\mathcal{A},\mathcal{B}} = \zeta_j \; b(u_j, v) \; , & \text{for all} \quad v \in \mathcal{H} \\ \|u_j\|_{0,\mathcal{B}} \quad\quad = 1 \; . & \end{array}\right\} \tag{19}$$

It is self-evident that the eigenpairs of (12) and (19) are in one-one correspondence. In fact, (λ_j, u_j) is an eigenpair of (12) if and only if (ζ_j, u_j), with $\zeta_j = \lambda_j + \sigma$, is an eigenpair of (19). Now, because the Hermitian form $(\cdot,\cdot)_{\kappa,\mathcal{A},\mathcal{B}}$ is continuous and coercive, we have that the solution operator is compact and then using the spectral theorem for compact operators it yields that the spectrum of (19) consists of eigenvalues of finite multiplicity, see [7]. The same result holds also for (12) due to the correspondence between the spectra of the two problems.

The distance of an approximate eigenfunction from the true eigenspace is a crucial quantity in the convergence analysis for eigenvalue problems especially in the case of non-simple eigenvalues.

Definition 1 Given a function $v \in L^2(\Omega)$ and a finite dimensional subspace $\mathcal{P} \subset L^2(\Omega)$, we define:

$$\text{dist}(v, \mathcal{P})_{0,\mathcal{B}} \; := \; \min_{w \in \mathcal{P}} \|v - w\|_{0,\mathcal{B}} \; .$$

Similarly, given a function $v \in H^1(\Omega)$ and a finite dimensional subspace $\mathcal{P} \subset H^1(\Omega)$, we define:

$$\text{dist}(v, \mathcal{P})_{\kappa,\mathcal{A},\mathcal{B}} \; := \; \min_{w \in \mathcal{P}} \|v - w\|_{\kappa,\mathcal{A},\mathcal{B}} \; ,$$

where $\|\cdot\|_{\kappa,\mathcal{A},\mathcal{B}}$ is defined in Lemma 1.

Now let λ_j be any eigenvalue of (12), let $E(\lambda_j)$ denote the finite dimensional space spanned by the eigenfunctions of λ_j and set $E_1(\lambda_j) = \{u \in E(\lambda_j) : \|u\|_{0,\mathcal{B}} = 1\}$. Let T_{λ_j} denote the orthogonal projection of H^1 onto $E(\lambda_j)$ with respect to the inner product $(\cdot,\cdot)_{\kappa,A,B}$ defined in (18). The following lemma is proved in [19, Lemma 3.3].

Lemma 2 *Let* $(\lambda_{j,n}, u_{j,n})$ *be an eigenpair of* (16). *Then*

$$\|u_{j,n} - u_j\|_{0,\mathcal{B}} = \text{dist}(u_{j,n}, E_1(\lambda_j))_{0,\mathcal{B}} \; , \tag{20}$$

if and only if

$$\|u_{j,n} - u_j\|_{\kappa,\mathcal{A},\mathcal{B}} = \text{dist}(u_{j,n}, E_1(\lambda_j))_{\kappa,\mathcal{A},\mathcal{B}} \; . \tag{21}$$

4 Residual based error estimator

Our a posteriori error estimator presented in (22) below is based on the results in [28] (for $\alpha = 0$, in the notation of that paper) that we extended to the PC case. The most important characteristic of the error estimator is reliability, which in broad terms means that the ratio of the actual error to the error estimator is bounded above by a positive constant independent of the mesh. As in [28], it is possible to define error estimators for PCs for $\alpha \neq 0$, but in order to keep the exposition simple, we decided to consider only the case $\alpha = 0$. As already explained in [28], a p-independent proof for the efficiency of the error estimator is still not available in the case when $\alpha = 0$ due to the p-dependence of polynomial inverse estimates. In a similar way as in [28] it is possible also with our error estimator to prove the efficiency independent of h, but still p-dependent. Nevertheless, as in [28], our numerical experiments in Section 5 suggest that our error estimator is also efficient in p. Moreover, this error estimator can be considered as the extension to the hp-case of the error estimator presented in [19], which was only designed for h-adaptive finite element methods.

Notation 1 *From now on, we write $A \lesssim B$ when A/B is bounded above by a constant independent of n, the size of the elements and the order of polynomials used within the elements. The notation $A \cong B$ means $A \lesssim B$ and $A \gtrsim B$.*

The residual estimator $\eta_{j,n}$ is defined as a sum of element residuals and edge residuals, which are all computable quantities. For $f \in \mathcal{F}(\mathcal{T}_n)$, we denote by $\tau_1(f)$ and $\tau_2(f)$, the two elements sharing $f \in \mathcal{F}(\mathcal{T}_n)$.

We let $\mathbf{n}_f$ denote the unit normal on the edge f, which is assumed to point from $\tau_1(f)$ into $\tau_2(f)$. To simplify the notation, we define the map $[\cdot]_f$ as follows

Definition 2 We can define for any function $g : \Omega \to \mathbb{C}$ which is continuous on each element of the mesh $\mathcal{T}_n$ and for any $f \in \mathcal{F}(\mathcal{T}_n)$

$$[g]_f(x) := \left(\lim_{\substack{\tilde{x}\in\tau_1(f)\\ \tilde{x}\to x}} g(\tilde{x}) \;-\; \lim_{\substack{\tilde{x}\in\tau_2(f)\\ \tilde{x}\to x}} g(\tilde{x}) \right), \quad \text{with } x \in f \ .$$

Definition 3 (Residual Estimator) The definition of the residual estimator $\eta_{j,n}$ involves two maps: $R_I(\cdot,\cdot)$, which expresses the contributions from the elements in the mesh:

$$R_I(u,\lambda)(x) := \big((\nabla + i\kappa)\cdot\mathcal{A}(\nabla + i\kappa)u \;+\; \lambda\mathcal{B}u\big)(x), \quad \text{with } x \in \mathrm{int}(\tau), \quad \tau \in \mathcal{T}_n,$$

where $\mathrm{int}(\tau)$ is the interior of the element τ and $R_F(\cdot)$, which expresses the contributions from the edges of the elements:

$$R_F(u)(x) := \big[\mathbf{n}_f \cdot \mathcal{A}(\nabla + i\kappa)u\big]_f(x), \quad \text{with } x \in \mathrm{int}(f), \quad f \in \mathcal{F}(\mathcal{T}_n) \ .$$

(Recall that the jumps of the coefficients are assumed to be aligned with the meshes.)

Then the residual estimator $\eta_{j,n}$ for the computed eigenpair $(\lambda_{j,n}, u_{j,n})$ is defined as:

$$\eta_{j,n} := \left\{ \sum_{\tau\in\mathcal{T}_n} \frac{h_\tau^2}{p_\tau^2}\beta_\tau^{-1}\|R_I(u_{j,n},\lambda_{j,n})\|_{0,\tau}^2 \; + \sum_{f\in\mathcal{F}(\mathcal{T}_n)} \frac{h_f}{p_f}\beta_f^{-1}\|R_F(u_{j,n})\|_{0,f}^2 \right\}^{1/2}, \tag{22}$$

where $\beta_\tau := \mathcal{A}_{\max}|_\tau$, $\beta_f := \max\{\mathcal{A}_{\max}|_{\tau_1(f)}, \mathcal{A}_{\max}|_{\tau_2(f)}\}$, and $\mathcal{A}_{\max}$ denotes the maximum eigenvalue of $\mathcal{A}$.

In order to prove the reliability we use the interpolation results presented in [29] where two interpolation operators are introduced. Firstly, we have the Clément type interpolation operator [29, Theorem 3.1] that we are going to use for the full-periodic case. Secondly, we have the Scott-Zhang type interpolation operator [29, Theorem 3.3] that, since it is able to handle homogeneous boundary conditions, we are going to use in the semi-periodic case to approximate surface modes. In order to simplify the notation, we are going to denote both interpolation operators with $I_n : \mathcal{H} \to S_{\underline{p}}(\mathcal{T}_n, \Omega)$, where the actual definition of the operator depends on the case under consideration. Coming from [29] we have that both interpolation operators satisfy:

$$\|v - I_n v\|_{0,\tau} \lesssim \frac{h_\tau}{p_\tau}\|v\|_{1,\omega(\tau)}, \qquad \text{and} \qquad \|v - I_n v\|_{0,f} \lesssim \left(\frac{h_f}{p_f}\right)^{\frac{1}{2}}\|v\|_{1,\omega(f)} , \tag{23}$$

where $\omega(\tau)$ (respectively $\omega(f)$) denotes the union of all elements sharing at least a vertex with τ (resp. f) .

Theorem 2 (Reliability for eigenfunctions) *Let $(\lambda_{j,n}, u_{j,n})$ be a computed eigenpair with $\lambda_{j,n}$ converging to an eigenvalue λ_j of (12). Then*

$$\mathrm{dist}(u_{j,n}, E_1(\lambda_j))_{\kappa,\mathcal{A},\mathcal{B}} \;\lesssim\; \eta_{j,n} \;+\; G_{j,n}, \tag{24}$$

where

$$G_{j,n} \;=\; \frac{1}{2}(\lambda_j + \lambda_{j,n} + 2\sigma)\frac{\mathrm{dist}(u_{j,n}, E_1(\lambda_j))_{0,\mathcal{B}}^2}{\mathrm{dist}(u_{j,n}, E_1(\lambda_j))_{\kappa,\mathcal{A},\mathcal{B}}}. \tag{25}$$

The proof of Theorem 2 is the same as the proof of reliability for eigenfunctions in [19], with the only difference that in this case the two interpolation operators introduced in [29] are used.

The next theorem, already presented in [19], shows the reliability for eigenvalues.

Theorem 3 (Reliability for eigenvalues) *Under the same assumptions as in Theorem 2, we have:*

$$|\lambda_{j,n} - \lambda_j| \;\lesssim\; \eta_{j,n}^2 \;+\; G'_{j,n} \;,$$

where

$$G'_{j,n} = \frac{1}{2}\eta_{j,n}(\lambda_j + \lambda_{j,n} + 2\sigma)\frac{\mathrm{dist}(u_{j,n}, E_1(\lambda_j))^2_{0,\mathcal{B}}}{\mathrm{dist}(u_{j,n}, E_1(\lambda_j))_{\kappa,\mathcal{A},\mathcal{B}}}$$

$$+ \frac{1}{2}(\lambda_{j,n} - \lambda_j + 2\sigma)\mathrm{dist}(u_{j,n}, E_1(\lambda_j))^2_{0,\mathcal{B}} \ .$$

5 Adaptive FEM and numerical experiments

In this section we have collected numerical results using our a posteriori error estimator with the clear aim to show the robustness of the error estimator and the fast decay of the error on a sequence of *hp*-adapted meshes. In all examples we solved the TE case because it is harder to solve, since localized singularities in the gradient of the eigenfunctions are probable to appear due to the discontinuous coefficient in the second order term.

Following [6], we assume an error model of the form

$$\lambda_{j,h} = \lambda_j + Ce^{-2\gamma\sqrt[3]{\mathrm{DOFs}}},$$

for problems with discontinuous coefficients, whose eigenfunctions are expected to have isolated singularities. The constants C and γ are determined by least-squares fitting, and γ is reported for each problem.

Plots are given of the error for eigenvalues, the correspondent value of the a posteriori error estimator and the associated effectivity index, which is defined as $|\lambda_{j,n} - \lambda|/\eta^2_{j,n}$. For comparison we plots the convergence curves from both the *h*-adaptive method and the *hp*-adaptive method and we denote the errors with "error-*h*" and "error-*hp*" respectively. Similarly we denote the values of the error estimator for the *h*-case and *hp*-case with a "post-*h*" and a" post-*hp*" respectively. In order to visually appreciate the converge rate of the *hp*-adaptive method, we plot a red line computed with the least-squares fitting method to highlight the slope of the curve.

As reference solutions for problems in this section we use highly accurate computations on very rich finite element spaces to produce "exact eigenvalues" for our comparisons.

First of all we would like to illustrate with an example of how to compute the spectrum of a PC. The spectra of photonic crystals typically contain band gaps, but, for many applications, the identification of band gaps is not enough. Commonly it is necessary to perturb artificially the spectrum by modifying the geometry of the crystal. Probably the most common alteration is the creation of eigenvalues inside the gaps in the spectra of the media. The importance of these eigenvalues is due to the fact that electromagnetic waves, which have frequencies corresponding to those eigenvalues, may remain trapped inside the crystal [15,17]. The common way to create such eigenvalues is by introducing a localized defect in the periodic structures — see [17] and [16, Theorem 2]. Such localized defects do not change the bands of the essential spectrum [16, Theorem 1]. For sake of brevity we are going to consider only the TE case

in this example. In this case $\mathcal{A}$ is piecewise constant, $\mathcal{B} = 1$ and there are typically localized singularities in the gradient of the eigenfunctions at corner points of the interface in $\mathcal{A}$ (from discontinuities in the dielectric ε), leading to a strong need for adaptivity.

The first step in order to analyze a PC is to compute the band structure of the periodic structure of the crystal. In this example we consider a square unit cell with a square inclusion of side 0.5 centered inside it. We choose $\mathcal{A}$ to take the value 1 outside the inclusion and the value 0.05 inside it, see Figure 2(a). This is a realistic example, since expected jumps in dielectric permittivity of about this order have been already considered, see [20]. Moreover an higher jump in dielectric permittivity can make the problem numerically harder to solve due the fact that stronger singularities could appear.

Due to symmetries in the problem, in order to produce accurately the band structure of the crystal it is just necessary to compute the eigenvalues of (1) for the values of κ in the reduced Brillouin zone, see Figure 2(b), instead of using the entire first Brillouin zone.

Each eigenvalue of (1) can be seen as a function of the quasimomentum $\lambda_j(\kappa)$, in this way we can obtain the plot in Figure 3(a), where we have plotted just the first four bands and for sake of clarity we just considered the values of κ on the border of the reduced Brillouin zone (we used Γ to parametrize the contour of the reduced Brillouin zone). As can be seen the minimum and the maximum of each function $\lambda_j(\kappa)$ delimit a band of the spectrum and between bands sometimes gaps can be found. The frequencies of light corresponding to points in the gap are not allowed to travel across the periodic structure of the PC. In this example it seems that there is a gap between the first and the second band. To be sure of that it is necessary to compute the entire bands. In Figure 3(b) the first three bands are plotted over the Brillouin zone. The figure confirms that between the first and the second band there is a gap. The surfaces in Figure 3(b) are computed with Algorithm 3 in [18], which is particularly efficient in computing entire bands.

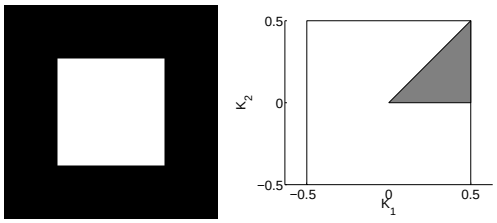

(a) (b)

Fig. 2 (a) Structure of the primitive cell. (b) The dark triangle is the reduced Brillouin zone for the primitive cell in (a).

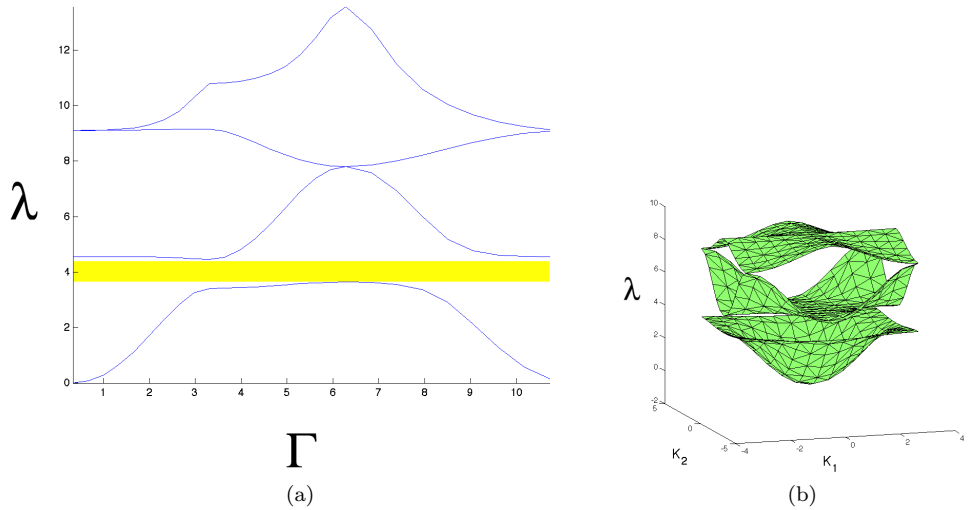

Fig. 3 (a) Band structure of the spectrum for the periodic crystal. The gap between the first two bands has been highlighted in yellow. (b) Band structure of the spectrum for the periodic crystal.

As predicted by the theory [23], the presence of a compact defect in the periodic structure can consequently create localized eigenvalues in the gaps that correspond to trapped modes. These modes can travel in the z-direction of the PC with almost no losses. A frequently used way to search for these trapped mode is to consider the super-cell framework [36], in which the considered primitive cell (called super-cell) is a portion of the periodic structure including the defect. Due to the periodic boundary conditions, the defect is not any more compact because it is repeated in each super-cell, see Figure 4(a) for a plot of the super-cell with a defect. The introduction of the defect in the super-cell does not lead to the creation of eigenvalues in the gaps, but it could create narrow new bands in the gaps which shrink exponentially fast to eigenvalues when the number of layers of periodic structure around the defect in the super-cell is increased [36]. Computing the band structure of the super-cell we obtain Figure 4(b) where a new narrow band of index $j = 25$ is now present in the first gap.

The preferable way to numerically discover these trapped mode is first to compute the position of the gaps in the spectrum of the periodic structure with no defects and then check in the super-cell for the presence of any band in the span of the already identified gaps for the periodic structure.

This way to proceed, that could seem rather complicated, is numerically efficient because the localization of the gaps is done on the single cell problem, that is a small problem to solve. Then on the super-cell with the defect, only the eigenvalues in the gaps are computed. That could be easily done using the

shift and invert spectral transformation in ARPACK [24] and setting the shift value to the middle point of a gap.

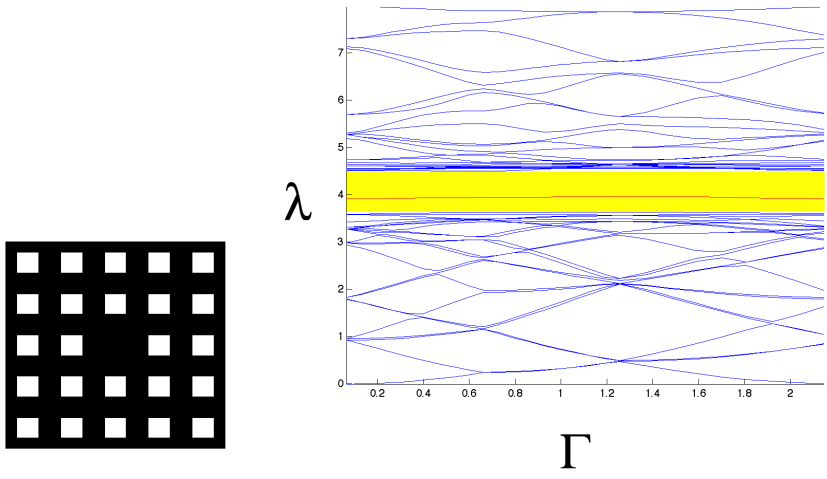

(a) (b)

Fig. 4 (a) Structure of the super-cell with a defect in the center. (b) Band structure of the spectrum for the supecell in (a). The first gap has been highlighted in yellow and the newly created trapped band in red.

Algorithm 1 *hp*-adaptive algorithm

$(\lambda_{j,n}, u_{j,n}) := \text{Adapt}(\mathcal{T}, S_{\underline{p}}(\mathcal{T}, \Omega), j, \theta, \text{tol})$
$n := 1$
$\mathcal{T}_1 := \mathcal{T}$
repeat
  Compute the j-th eigenpair $(\lambda_{j,n}, u_{j,n})$ on $\mathcal{T}_n$
  Compute $\eta_{j,\tau}$ for all $\tau \in \mathcal{T}_n$
  if $\left(\sum_{\tau\in\mathcal{T}_n} \eta_{j,\tau}^2\right)^{1/2} < \text{tol}$ **then**
    exit
  else
    $(\mathcal{T}_{n+1}, S_{\underline{p}}(\mathcal{T}_{n+1}, \Omega)) := \text{Refine}(\mathcal{T}_n, S_{\underline{p}}(\mathcal{T}_n, \Omega), \theta, \eta_j)$
    $n := n + 1$
  end if
until

All the experiments have been carried out using AptoFEM (`www.aptofem.com`) on a single processor desktop machine. In particular, we used ARPACK [24] to compute the eigenvalues and MUMPS [2] to solve the linear systems. The algorithm used to compute all numerical results in this

section is presented in Algorithm 1, which takes as input: an initial mesh $\mathcal{T}$, an initial finite element space $S_{\underline{p}}(\mathcal{T}, \Omega)$, the index j of the eigenpair to approximate, a real value $0 \leq \theta \leq 1$ to tune the fixed-fraction marking strategy and finally a real and positive value tol which prescribes the required tolerance. The algorithm has a very simple structure that consists of a repeat-until loop. During each iteration of the loop a new approximation of the eigenpair of interest is computed, then the error estimator is calculated and, if the estimated error $\left(\sum_{K\in\mathcal{T}} \eta_{j,K}^2\right)^{1/2}$ is smaller than the prescribed tolerance tol the algorithm stops; otherwise the mesh $\mathcal{T}$ and the space $S_{\underline{p}}(\mathcal{T}, \Omega)$ are refined and another iteration follows. The function Refine applies a simple fixed-fraction strategy to mark a minimal subset of elements containing a portion of the error proportional to θ. Then the choice for each marked element between splitting the element into smaller elements using red-refinement (h-refinement) or increasing the polynomial order (p-refinement) is made by testing the local analyticity of the solution in the interior of the element as described in [13]. In the case that we are only interested in using h-refinement the local analyticity test can be avoided. In order to avoid the presence of hanging nodes in the refined meshes, the Refine procedure also closes the meshes using green-refinement, i.e. the hanging nodes are removed applying extra refinements.

5.1 TE mode problem on crystal with point defect

Now we pursue the approximation of a trapped mode in Figure 4(b). In order to do this we are now considering the super-cell in Figure 4(a) as the domain of our problem. Since the domain is $(-2.5, 2.5)^2$, it comes that the first Brillouin zone is: $(-\pi/5, \pi/5)^2$. We compared h- with hp-adaptivity for different values of the quasimomentum for the 28th smallest eigenvalue which seems to be the trapped mode.

Figures 5(a), 5(b) and 5(c) contain the convergence plots for the eigenvalue of the trapped band for different values of quasimomentum. It is possible to see that in all cases with the hp-adaptivity the convergence is much faster than with only h-adaptivity and always seems exponential with values of γ: 0.08455, 0.09540 and 0.96318.

In Figure 6(a) we depict the mesh coming from the seventh iteration of Algorithm 1, as can be seen there is a lot of refinement around the defect, especially around the corners of the inclusions closest to the defect. Away enough from the defect the corners of the inclusions are not refined much. Since the trapped mode has a fast decay away from the defect, this prevents any strong singularity to appear in the corners of the inclusions far enough from the defect. This is the reason why the refinement is so concentrated near the defect and why the corners of the inclusions away from the defect seem not to show important singularities. In Figure 6(b) we depict the eigenfunction corresponding to the trapped eigenvalue with quasimomentum $\kappa = (0, 0)$.

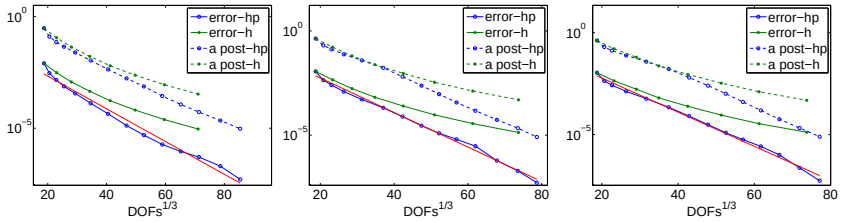

Fig. 5 (a) Convergence plots for the super-cell problem for quasimomentum $(0, 0)$. (b) Convergence plots for the super-cell problem for quasimomentum $(\pi/5, 0)$. (c) Convergence plots for the super-cell problem for quasimomentum $(\pi/5, \pi/5)$.

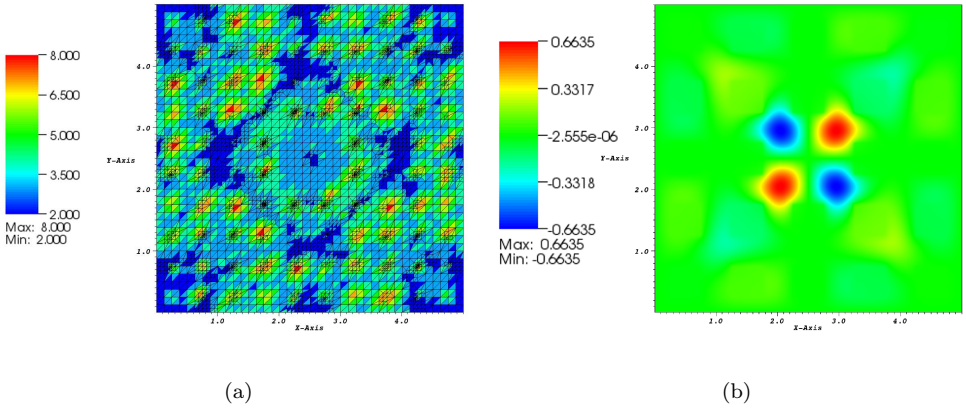

Fig. 6 (a) An adapted mesh for a trapped eigenvalue of the TE case problem on a super-cell with quasimomentum $\kappa = (0, 0)$. The color scale indicates the polynomial order in the elements. (b) A picture of the eigenfunction trapped in the defect of the TE case problem on a super-cell with quasimomentum $\kappa = (0, 0)$.

5.2 TE mode problem on crystal with line defect

In this section we approximate a trapped mode in a PC waveguide, which is constructed by removing a column of rods. Waveguides with similar geometry have been already considered in [27]. Numerically we approximate the 6th smallest eigenvalue of the problem by considering the super-cell in Figure 7(a).

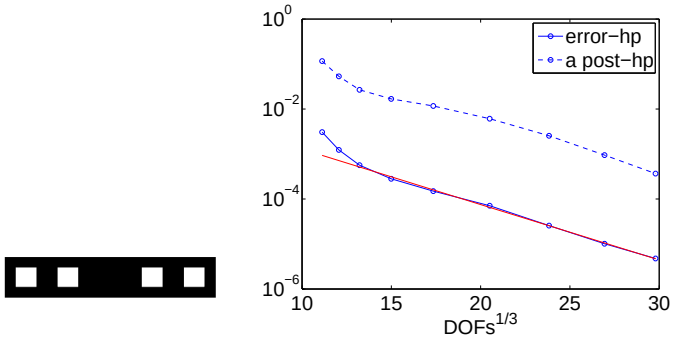

(a) (b)

Fig. 7 (a) Super-cell domain for the problem on crystal with line defect. (b) Convergence plots for the line defect problem for quasimomentum $(0, 0)$.

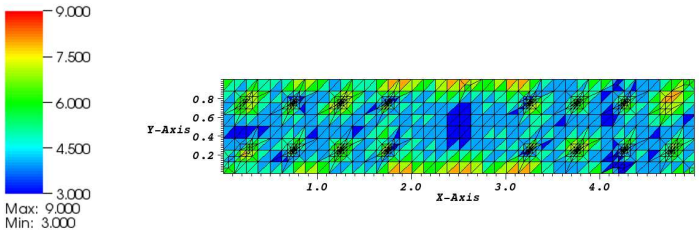

(a)

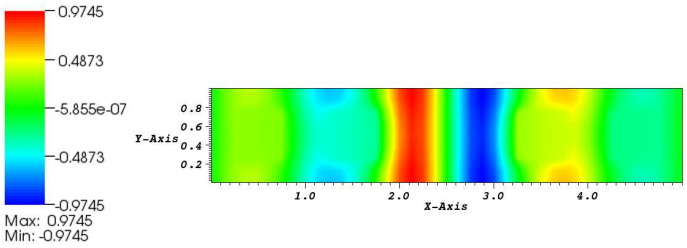

(b)

Fig. 8 (a) An adapted mesh for a trapped eigenvalue of the TE case for the line defect problem with quasimomentum $\kappa = (0, 0)$. The color scale indicates the polynomial order in the elements. (b) A picture of the eigenfunction trapped in the line defect of the TE case problem with quasimomentum $\kappa = (0, 0)$.

Figure 7(b) contains the convergence plot for a trapped mode with $\kappa = (0,0)$ and using *hp*-adaptivity, which as before seems exponential with $\gamma = 0.14167$.

In Figure 8(a) we depict the mesh coming from the ninth iteration of Algorithm 1. In Figure 8(b) we depict the eigenfunction corresponding to the eigenvalue trapped in the gap with quasimomentum $\kappa = (0,0)$.

5.3 TE mode problem on V-bend crystal

This section is dedicated to the approximation of a trapped mode in a V-bend waveguide. The trapped modes in the bend are important in practice because exciting these modes it is possible to make an electromagnetic wave to go around a bend. Waveguides with similar geometry have been already considered in [27]. Numerically we approximate the 3rd smallest eigenvalue with a shift of 0.84 in the shift and invert spectral transformation in ARPACK and we considered the super-cell in Figure 1(c) as the domain of the problem.

Figure 9 contains the convergence plot for a trapped mode with $\kappa = (0,0)$ and using *hp*-adaptivity, which as before converges exponentially with $\gamma = 0.053359$.

In Figure 10(a) we depict the mesh coming from the sixth iteration of Algorithm 1. In Figure 10(b) we depict the eigenfunction corresponding to the eigenvalue in the bend with quasimomentum $\kappa = (0,0)$.

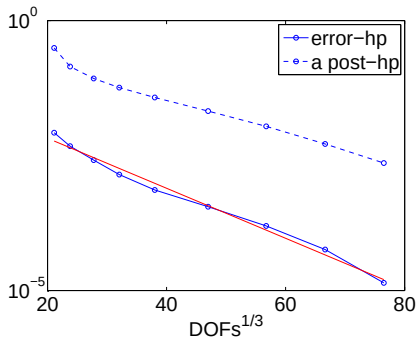

Fig. 9 Convergence plots for the V-bend problem for quasimomentum $(0,0)$.

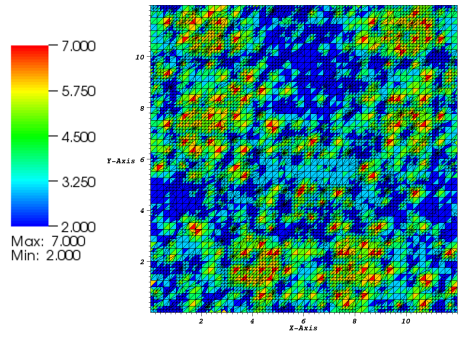

(a)

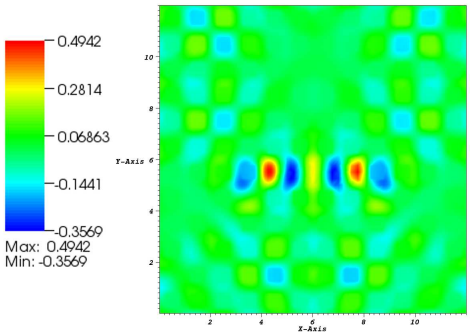

(b)

Fig. 10 (a) An adapted mesh for a trapped eigenvalue of the TE case for the V-bend problem with quasimomentum $\kappa = (0, 0)$. The color scale indicates the polynomial order in the elements. (b) A picture of the eigenfunction trapped in the V-bend of the TE case problem with quasimomentum $\kappa = (0, 0)$.

5.4 TE mode problem on the surface of a photonic crystal

In this section we approximate a mode localized on the surface of a semi-infinite PC. In order to make the computation possible we truncate the domain in the horizontal direction and apply periodic boundary conditions in the vertical direction only. The considered domain is $(-10, 10) \times (-0.5.0.5)$. Because the variational formulation of the problem comes from applying the Floquet transform only in the y-direction, the corresponding Brillouin zone is $\{0\} \times (-\pi, \pi)$. Surface modes have been already considered in [20], where it is also noticed that in order to make such modes more likely to appear, the surface of the crystal should be made by truncating the periodic medium cutting a column of

rods in half, see Figure 11(a). Numerically we approximate the 60th smallest eigenvalue of the problem.

(a)

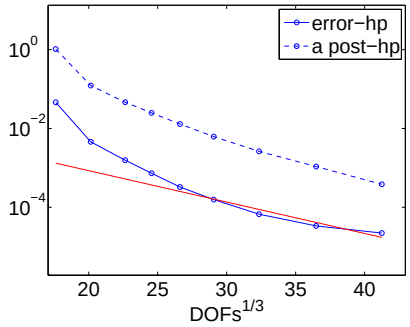

(b)

Fig. 11 (a) Domain for the problem on the surface of a semi-infinite PC. (b) Convergence plots for the surface problem for quasimomentum $(0, 0)$.

Figure 11(b) contains the convergence plot for the surface mode with $\kappa = (0, 0)$ and using *hp*-adaptivity, with $\gamma = 0.064134$.

In Figure 12 we depict the mesh coming from the sixth iteration of Algorithm 1. In Figure 13 we depict the corresponding eigenfunction with quasimomentum $\kappa = (0, 0)$.

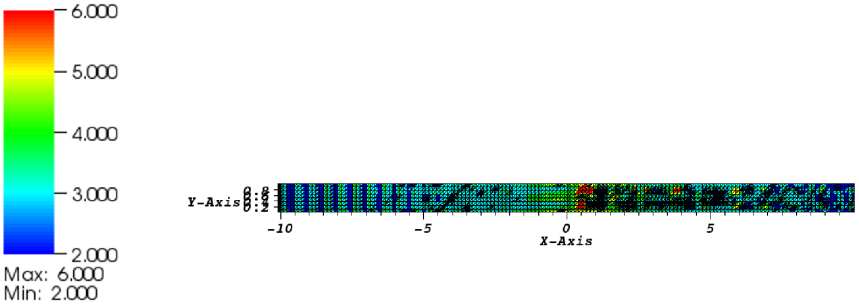

Fig. 12 An adapted mesh for a trapped eigenvalue of the TE case for the surface problem with quasimomentum $\kappa = (0, 0)$. The color scale indicates the polynomial order in the elements.

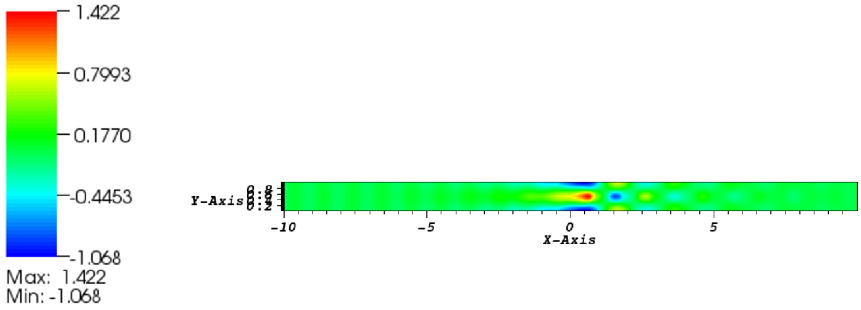

Fig. 13 A picture of the eigenfunction trapped in the surface of the TE case problem with quasimomentum $\kappa = (0, 0)$.

References

1. M. Ainsworth and J. Oden. *A Posterior Error Estimation in Finite Element Analysis*. Wiley, New York, 2000.
2. P. Amestoy, I. Duff, and J.-Y. L'Excellent. Multifrontal parallel distributed symmetric and unsymmetric solvers. *Comput. Methods in Appl. Mech. Eng.*, 184(2–4):501–520, 2000.
3. H. Ammari and F. Santosa. Guided waves in a photonic bandgap structure with a line defect. *SIAM J. Appl. Math.*, 64(6):2018–2033, 2004.
4. N. W. Ashcroft and N. D. Mermin. *Solid State Physics*. Saunders College, Philadelphia, 1976.
5. W. Axmann and P. Kuchment. An efficient finite element method for computing spectra of photonic and acoustic band-gap materials. *J. Comput. Physics*, 150:468–481, 1999.
6. I. Babuška and B. Q. Guo. The h-p version of the finite element method for domains with curved boundaries. *SIAM J. Numer. Anal.*, 25(4):837–861, 1988.
7. I. Babuka and J. Osborn. Eigenvalue problems. *in Handbook of Numerical Analysis Vol II, eds P.G. Cairlet and J.L. Lions, North Holland*, pages 641–787, 1991.
8. M. S. Birman and T. A. Suslina. A periodic magnetic hamiltonian with a variable metric. the problem of absolute continuity. *Petersburg Math J.*, pages 10–5, 1999.
9. D. Boffi, M. Conforti, and L. Gastaldi. Modified edge finite elements for photonic crystals. *Numer. Math.*, 105:249–266, 2006.
10. Y. Cao, Z. Hou, and Y. Liu. Convergence problem of plane-wave expansion method for phononic crystals. *Phys Lett A*, 327:247–253, 2004.
11. D. C. Dobson. An efficient method for band structure calculations in 2D photonic crystals. *J. Comp. Phys.*, 149:363–376, 1999.
12. D. C. Dobson, J. Gopalakrishnan, and J. E. Pasciak. An efficient method for band structure calculations in 3D photonic crystals. *J. Comp. Phys.*, 161(2):668–679, 2000.
13. T. Eibner and J. M. Melenk. An adaptive strategy for hp-FEM based on testing for analyticity. *Comput. Mech.*, 39(5):575–595, 2006.
14. C. Engström and M. Wang. Complex dispersion relation calculations with the symmetric interior penalty method. *Int. J. Numer. Meth. Eng.*, 84(7):849–863, 2010.
15. A. Figotin and V. Gorentsveig. Localized electromagnetic waves in a layered periodic dielectric medium with a defect. *Phys. Rev. B*, 58(1):180–188, 1998.
16. A. Figotin and A. Klein. Localized classical waves created by defects. *J. Stat. Phys.*, 86:165–177, 1997.
17. A. Figotin and A. Klein. Midgap defect modes in dielectric and acoustic media. *SIAM J. Appl. Math.*, 58(6):1748–1773, 1998.
18. S. Giani. Convergent adaptive finite element methods for photonic crystal applications. *Math. Mod. and Meth. in App. Sci. (M3AS)*, 22(10):2018–2033, 2012.

19. S. Giani and I. G. Graham. Adaptive finite element methods for conputing band gaps in photonic crystals. *Num. Math.*, 121(1):31–64, 2011.
20. J. Joannopoulos, S. Johnson, J. Winn, and R. Meade. *Photonic Crystals: Molding the Flow of Light*. Princeton University Press, Singapore, 2nd revised edition edition, 2008.
21. S. G. Johnson and J. D. Joannopoulos. Block-iterative frequency-domain methods for Maxwell's equations in a planewave basis. *Opt. Express*, 8:173–190, 2001.
22. P. Kuchment. *Floquet Theory for Partial Differential Equations*. Birkhauser Verlag, Basel, 1993.
23. P. Kuchment. The mathematics of photonic crystals. *SIAM, Frontiers Appl. Math.*, 22:207–272, 2001.
24. R. B. Lehoucq, D. C. Sorensen, and C. Yang. *ARPACK Users' Guide: Solution of Large Scale Eigenvalue Problems with Implicitly Restarted Arnoldi Methods*. SIAM, 1998.
25. Q. H. L. M. Luo and Z. Li. Spectral element method for band structures of two-dimensional anisotropic photonic crystals. *Phys. Rev. E*, 79, 2009.
26. M. Marletta. Eigenvalue problems on exterior domains and Dirichlet to Neumann maps. *J. Comput. Appl. Math.*, 171(1-2):367391, 2004.
27. A. Mekis, S. Fan, and J. D. Joannopoulos. Bound states in photonic crystal waveguides and waveguide bends. *Phys Rev B*, 58(8):4809–4817, 1998.
28. J. Melenk and B. Wohlmuth. On residual-based a posteriori error estimation in hp-FEM. *Adv. Comput. Math.*, 15(1):311–331–331, 2001.
29. J. M. Melenk. hp-interpolation of nonsmooth functions and an application to hp-a posteriori error estimation. *SIAM J. Numer. Anal.*, 43(1):127, 2005.
30. R. Norton and R. Scheichl. Convergence analysis of planewave expansion methods for 2D Schrödinger operators with discontinuous periodic potentials. *SIAM J. Numer. Anal.*, 47(6):4356–4380, 2010.
31. R. A. Norton and R. Scheichl. Planewave expansion methods for photonic crystal fibres. *Appl. Numer. Math.*, 2012.
32. G. J. Pearce, T. D. Hedley, and D. M. Bird. Adaptive curvilinear coordinates in a plane-wave solution of Maxwell's equations in photonic crystals. *Phys Rev B*, 71(19):195108–+, 2005.
33. K. Sakoda. *Optical Properties of Photonic Crystals*. Springer-Verlag, Berlin, 2001.
34. K. Schmidt and R. Kappeler. Efficient computation of photonic crystal waveguide modes with dispersive material. *Opt. Express*, 18(7):7307–7322, 2010.
35. K. Schmidt and P. Kauf. Computation of the band structure of two-dimensional photonic crystals with hp finite elements. *Comput. Meth. Appl. Mech. Eng.*, 198:1249–1259, 2009.
36. S. Soussi. Convergence of the supercell method for defect modes calculations in photonic crystals. *SIAM J. Numer. Anal.*, 43(3):1175–1201, 2005.